Supporting Information

Wagner et al. 10.1073/pnas.1012722107

SI Materials and Methods

Infrared Radiofluorescence Dating. ***Samples.*** Sample preparation was carried out in the luminescence laboratory under subdued red light. The first 2 to 3 cm of sediments at the front and back sides of the sampling tubes were removed to exclude any light-exposed material. These parts of the sample were used to determine the in situ and the saturation water contents of the sediments (Table S1). The procedure of K-feldspar extraction comprised sieving (different grain-size fractions between 100 and 315 μm), removal of carbonates (HCl) and organics (H_2O_2), feldspar flotation, heavy liquid (Na-polytungstate) density separation (2.53–2.58 g cm^{-3}), etching (HF, HCl) the α-affected outer layer of the grains, and final sieving. The samples Mau 1-1 and Mau 1-2 had to be treated as one sample in a second run because there was not sufficient K-feldspar in each of them. In addition, the mineral extraction procedure had to be repeated for other samples, partly using another grain size.

Dose rate. At Freiberg, Marinelli beakers (dried sample weight *ca.* 1 kg) and a p-type high purity germanium detector of 36% relative efficiency situated in a low-level background shielding plus an anticoincidence muon shielding-guard were used. This type of detector did not allow a check for possible disequilibria within the ^{238}U decay chain with sufficient reliability. A set of samples of the same material (approximately 100 g dry mass in cylindrical containers) was therefore additionally measured at Dresden. There the γ-spectrometer consists of a coaxial p-type Ge detector with a relative efficiency of 92% and enhanced front-side sensitivity in the low-energy range (CANBERRA XtRa). The detector as well as the surrounding shielding were particularly developed for low-background applications (1) and are regularly used for the analysis of low-level natural radioactivity. The spectrometer itself is installed at a depth of 110 m w.e. in a shielded measuring chamber (2).

In both laboratories, the following radioisotopes were used for the analysis: ^{238}U decay series: ^{234}Th (for ^{238}U), ^{230}Th, ^{214}Pb and ^{214}Bi (^{222}Rn successors, for ^{226}Ra), ^{210}Pb; ^{232}Th decay series: ^{228}Ac (for ^{228}Ra), ^{212}Pb, ^{212}Bi and ^{208}Tl (for ^{228}Th); and ^{40}K. No indication of radioactive disequilibria in the ^{238}U decay chain was found, according to analysis of ^{238}U, ^{226}Ra, and ^{210}Pb in the Felsenkeller laboratory. The larger uncertainties in the ^{40}K determination of these measurements are due to lower accuracy of the calibration standard. For the infrared radiofluorescence (IR-RF) age calculation the error-weighted mean was used. In case of horizon Mau 1 the value includes three measurements because both samples (Mau 1-1 and Mau 1-2), taken parallel in a distance of approximately 0.4 m, had to be used to get to a sufficient amount of K-feldspar for IR-RF dose determination. The data used for calculating the dose rate and IR-RF age are given in Table S1.

The cosmic dose rate (Table S2) was calculated according to a five-stage model with varying overburden using a set of roughly calculated IR-RF ages and further geochronologic information (e.g., the thermoluminescence ages of the overlying loess complex) (3). The software ADELE (see below) was used. The dose absorbed because of cosmic rays in five different periods of varying thickness and density of overburden was summed, and a mean cosmic dose-rate value was calculated. The value has a ±20% error, also to account for long-term variations in cosmic ray flux of the last 500,000 y (3). For clarity it should be mentioned that the influence of the cosmic ray dose rate on the age data is low, and a simpler procedure of its calculation would have been sufficient.

The internal dose rate of K-feldspar grains was calculated with 12.5% ± 0.5% K and the grain-size parameters, including etching and final sieving. Such a K-content can be applied because values in this range have been frequently measured in single aliquots (4). This value is also recommended in the literature (5). At a 95% confidence it covers 11.5–13.5% K-content. A further support for dose-rate calculations based on such K-concentrations is given by the fact that only K-feldspars emit IR-RF (i.e., the measured luminescence signal is strongly related to grains of K-rich feldspars). The stochiometric maximum of 14% is, however, rarely reached in nature. There was no access to analytical facilities to determine the K-content of 1- to 2-mg (single-aliquot) samples of the Mauer sediments during this study. This certainly would have led to a further lowering of the age errors. For other methods the amount of K-feldspar was too low, and the analysis of a bulk sample is not as valuable as that of the individual single aliquots used for dose determination. However, there is no risk of unreliable age data when using the above-mentioned K-contents together with the error quoted.

The water content of the sample was calculated from the saturation content determined in the laboratory. It can be assumed that until the sand quarrying started in the 19th century the Mauer sands were located below the groundwater table. The very good preservation of the fossils is a reliable indicator of such conditions. There are no indications for fluctuations of the groundwater table in the sediment sequence dated. Because the laboratory procedure probably overestimates the saturation water content slightly owing to higher packaging density of the sediment grains in the natural undisturbed sediments, 90% of the laboratory value is used, and 0.8 ± 0.2 of this value was applied for the dose-rate calculation. The moisture data are listed in Table S1.

In summary, we made conservative error estimates for all parameters of dose rate. It is of particular importance that the high internal dose-rate component, which also comprises a conservative error, makes the dose-rate values of all samples robust against any external influences. Although we did not find radioactive disequilibria in the recent state of the sediments, unknown disequilibria would have had small influence owing to the low radioactivity in the Mauer samples. For the calculation of the final dose rate of the Mauer sediments the software ADELE (*A*ge *DE*termination in *L*uminescence and *E*lectron Spin Resonance Dating) was used (6). It is based on the dose-rate conversion factors (7), radiation attenuation factors (8), and cosmic dose-rate calculation (3).

Equivalent dose. Determination of the equivalent dose was carried out with a single-aliquot regeneration technique (9). A laboratory-made radiofluorescence reader was used (10). The IRSAR (infrared radiofluorescence single-aliquot regeneration) protocol (11) comprises the measurements of the natural IR-RF signal and the regeneration dose characteristics after artificial optical bleaching by light of a solar simulator. Each aliquot carried a monolayer of K-feldspar grains (for grain size see Table S2) with a diameter of 6 mm (approximately 1 to 2 mg). Ten to twenty aliquots were measured per sample to account for identification of inhomogeneous reset of the IR-RF signal at the time of deposition. A stretched single exponential fit was applied to the regeneration dose characteristics. The results are listed in Table S2. Examples are given in Fig. S1.

To check the validity of the assumption that the aliquot size is not affected to a significant degree by intergrain variability within a mixed-grain population, it would have been helpful to also measure much smaller sample aliquots (i.e., <<6 mm diameter) or single grains. This was not possible with our RF-reader because a complete irradiation calibration (10 Cs sources) would be necessary for each individual single aliquot size, but the signal to noise ratio would be too low in such case.

Although at the Freiberg Laboratory optically stimulated luminescence (OSL) dose determination of feldspar or quartz grains can be carried out, it was not applied in this study. Despite the relatively low radioactivity in the "Mauer sands," the quartz OSL signal is in saturation at much lower ages than minimum ages of the site given (7). Feldspar OSL dating techniques suffer from signal fading and age underestimation if no corrections are made. Such correction methods are internationally under developement, but at the moment they are reliable just for linear signal growth (i.e., much younger sediments than the ones at the Mauer site).

Age calculation and errors. We applied an age statistic instead of an equivalent-dose statistic, because parallel samples investigated have their own individual radioisotope and water content (Table S1) or, for example in the case of Mau 3-1, different dose rates have to be applied in age calculation owing to different grain-size fractions (Table S2) used for the IR-RF equivalent-dose determinations. Thus a single-aliquot dose statistic, often used in luminescence dating of sediments, would have been possible just for Mau 1, 4, and 6 and would have failed for the other samples because different dose values are caused by different dose rates.

Single-aliquot or single-grain statistics is carried out commonly to reduce errors arising from incomplete reset of the luminescence signal at the time of deposition, although, of course, other sources of error can be reduced by determination of a large number of equivalent dose or age data, respectively. Much progress comes from investigations on data obtained in OSL dating of quartz using a single-aliquot regenerative dose protocol (12–14). All these methods cannot be directly applied to IR-RF dating. The main reason is that the error sources in dose determination are quite different. This is especially due to the low dynamic range of the IR-RF vs. dose–response characteristics (≈2 only; i.e., the IR-RF signal at zero dose is twice that of saturation dose, independent of whether an individual feldspar grain has high or low signal), which always decay exponentially (Fig. S1*A*). Thus, the relative errors of IR-RF equivalent doses increase with dose, even if any relative random dose errors are constant. The application of complex age models (15) fails owing to the relatively small number of measurements (16). Except for Mau 1 (10 data; small amount of K-feldspar fraction), 18–20 ages were determined in each horizon. It should be mentioned that the required IR-RF measurement time is in the range of 12–14 d per 10 aliquots in the case of such old sediments as at Mauer (i.e., 4 to 5 mo pure machine time for the 108 single-aliquot dose determinations of this study). Formerly published ages are mostly based on sets of five data; and with such a small number satisfactory results have been obtained. The IR-RF age data presented here are based on a much higher number of single-aliquot measurements. However, there is no systematic study for single-aliquot IR-RF age statistics. Necessarily, we applied a different statistical method for the analysis of the single-aliquot age data.

There is striking evidence of a broad age distribution, which also includes maximum ages larger than 2,000 ka but at a low frequency (Fig. S2). We thus had to extract those single-aliquot ages that do reflect the "true age." The main reason for overestimated ages is an incomplete reset of the luminescence signal at the time of deposition (incomplete bleaching). In a study on freshly deposited sediments, a distribution of IR-RF dose residuals in the range of approximately 0–50 Gy was obtained (8). The samples from fluvial environment ranged from approximately 1 to 50 Gy, but the highest value was determined on a flood loam (i.e., a type of sediment in which light-exposure during transport and deposition might have been very restricted). However, this worse case of 50 Gy would lead to a residual age of 20–33 ka in our samples, because the dose rate lies in the range of approximately 1.5–2.5 mGy a^{-1} (Table S2). This effect of "residual ages" especially occurs when the sediment is from a waterlain environment, compared with aeolian sediments, for which bleaching was much more effective owing to direct sunlight exposure. However, on the other hand one cannot assume that the lowest ages are the true values. Uncertainties in the entire measurement procedure, as well as variable bleaching, luminescence, and dosimetric parameters, will result in an age distribution of a more or less broad width for all well-bleached aliquots. Errors arising from variations in microdosimetry of the sediment grains may also play a significant role. However, this effect should be lower in our case because the major dose-rate component is the internal one arising from ^{40}K in K-feldspar, which lowers the influence of changes in the external radiation field. The latter problem is covered by the conservative error estimates of the dose rate.

The basic assumption of the applied statistical procedure is that the ages for a certain level of initial bleaching are normally distributed around an expected value. The whole age distribution then is the result of a convolution of the probability distribution of all bleaching levels with those normal distributions. The most completely reset signals then lead to ages forming the edge at the younger side of the total age distribution. First, from the age data of Table S3, histograms of the frequency distribution of ages within certain age intervals were derived (Fig. S2). The bin width was determined by the median of all total uncertainties of one dataset. For instance, a width of 107 ka was calculated for Mau 1. The bin width therefore changes from sample to sample. The lowest age of each dataset was used as the "younger" border of the first bar. There are some samples for which the first (youngest) bar is the highest: Mau 1, 3, 4, and 6. This bar was used for the further procedure as the representation of the distribution of all well-bleached aliquots. For Mau 2 and Mau 5, the distribution obviously involves more bars because at the younger side of the maximum a bin with lower frequency occurs. The classes used for further calculations are marked by arrows in Fig. S2. The mean ages of the samples were obtained by calculating the weighted mean of all included data using the inverse squared errors as weights. In Fig. S2 all data used for averaging are shown together with their errors. The weighted mean age x_0 is also given in the plots.

As a measure of the uncertainty of x_0, the width of the distribution of well-bleached aliquots (the variance σ^2) may serve. For this purpose the fraction of the total number of data was estimated, which was used for calculating the mean age x_0. The frequency of the first empty class at the younger side of the distribution is <1. Then the total number of unconsidered data is <2 for the sake of symmetry. If n is the number of considered data, $\frac{n}{n+2}$ is an estimation of the lower limit of that fraction of the total dataset that is involved in the analysis. The following estimate holds for an age interval [x_1; x_2] enclosing all interpreted, normally distributed data:

$$\int_{x_1}^{x_2} \frac{1}{\sqrt{2\pi}\cdot\sigma}\cdot e^{-\frac{1}{2}\cdot\frac{(x-x_0)^2}{\sigma^2}}dx = \frac{n}{n+2}.$$

From this equation the SD σ can be obtained from tabulated data of the standard normal distribution using $x_{1,2}$ values symmetrically to x_0. As an example, for Mau 2 both used bars contain 12 age values, the fraction of considered data are then $>\frac{12}{14} = 86\%$. The corresponding age interval of the bars is 516–682 ka. In a normal distribution, an interval including >86% of the total area belongs to a width of <2.9 σ. This leads to σ = 56 ka.

In Table 1 (main text) all age data are summarized that were obtained by the presented procedure. Furthermore, the normal distributions deduced from the x_0 σ values are presented in Fig. S2.

These distributions are estimates of the real ones for well-bleached samples. Because each single-aliquot age has a combined uncertainty from error propagation, and the resulting error, calculated as described above, includes the influence of the number of single-aliquot ages used, the error values given in Table 1 (main text) can be seen as SEs.

We have also tested other statistical methods, although, as mentioned above, there are restrictions in regard to the number of single-aliquot ages. These tests comprise procedures going along (becuase some modifications were necessary) the "leading edge" method (17), the age probability density distribution (18), and a calculation based on the median value. Because we cannot discuss the results to a full extent here, just two examples will be given. If we take the median value (which accounts simply for the skewed distribution) as upper age limit and calculate the age by the error-weighted mean of the lower 50% of the single-aliquot IR-RF ages, after they have passed a statistical test for outliers (Grubbs test), we get (Mau 1–6): 618 ± 30 ka, 595 ± 20 ka, 574 ± 19 ka, 518 ± 16 ka, 503 ± 13 ka, and 430 ± 12 ka. The mean ages and their SDs of all single-aliquot ages that form the "leading edge" (17) are (Mau 1–6): 616 ± 26 ka, 587 ± 47 ka, 567 ± 6 ka 502 ± 22 ka, 484 ± 23 ka, and 428 ± 23 ka. In summary, none of the six statistical methods further applied to the set of age data has given, in the range of errors, different results compared with those given in Table 1 (main text). Thus we have additional arguments that we could successfully reduce in our data the error of age overestimation due to the influence of insufficiently optical reset of the luminescence "clock" at the time of sediment deposition.

To get to a calculation of the age of the find horizon of *Homo heidelbergensis* based on the relevant IR-RF and electron spin resonance/U-series ages it was necessary to estimate to what extent the errors are random or systematic (11). As mentioned above, there is a systematic error of RF radiation source calibration in the calculation of the individual single-aliquot IR-RF ages (Table S3). We can assume 2%, using $Al_2O_3:C$, γ-irradiated in a certified facility (Sensor Technik und Elektronik Pockau-Lengefeld, Germany) for this purpose. Furthermore, variations of the moisture content may also be a source of systematic uncertainty of luminescence ages within a sample horizon (11). A change of the water content of 5% dry mass would lead to a change of approximately 15 ka of a 600 ka sample with radioactivity of Mau 1 or Mau 2 (i.e., an age error of 2.5%). The radioisotope concentration was determined in two independent laboratories using different calibration standards. Thus a systematic error in radioisotope determination arising from γ-spectrometry calibration need not be assumed. On the basis of this estimation we get for Mau 1 a random error $\sigma_r = 52$ ka and a systematic error $\sigma_s = 19$ ka and for Mau 2 $\sigma_r = 53$ ka and $\sigma_s = 19$ ka.

Electron Spin Resonance. U-series and electron spin resonance data obtained on Mauer teeth are shown in Tables S5 and S6, as well as in Fig. S3.

1. Köhler M, et al. (2009) A new low-level γ-ray spectrometry system for environmental radioactivity at the underground laboratory *Felsenkeller*. *Appl Radiat Isot* 67: 736–740.
2. Niese S, Köhler M, Gleisberg B (1998) Low-level counting techniques in the underground laboratory "Felsenkeller" in Dresden. *J Radioanal Nucl Chem* 233: 167–172.
3. Prescott JR, Hutton JT (1994) The cosmic ray contribution to dose rates for luminescence and ESR dating: Large depths and long-term variations. *Radiat Meas* 23: 497–500.
4. Dütsch C, Krbetschek MR (1997) New methods for a better K-40 internal dose rate determination. *Radiat Meas* 27:377–381.
5. Huntley DJ, Baril MR (1997) The K content of the K-feldspars being measured in optical dating or thermoluminescence dating. *Ancient TL* 15:11–13.
6. Kulig G (2005) *Preparation of a Software for Age Determination by Means of Luminescence Techniques* (Faculty of Mathematics Informatics, Technische Universität Freiberg, Germany) (in German).
7. Adamiec G, Aitken M (1998) Dose-rate conversion factors: update. *Ancient TL* 16: 37–50.
8. Brennan BJ (2003) Beta doses to spherical grains. *Radiat Meas* 37:299–303.
9. Preusser F et al. (2008) Luminescence dating: Basics, methods and application. *Quatern Sci J* 57:95–149.
10. Erfurt G, Krbetschek MR, Bortolot VJ, Preusser F (2003) A fully automated multi-spectral radioluminescence reading system for geochronometry and dosimetry. *Nucl Instrum Methods Phys Res* 207:487–499.
11. Erfurt G, Krbetschek MR (2003) IRSAR—a single-aliquot regenerative-dose dating protocol applied to the infrared radiofluorescence (IR-RF) of coarse-grain K feldspar. *Ancient TL* 21:21–28.
12. Murray AS, Wintle AG (2000) Luminescence dating of Quartz using an improved single aliquot regenerative dose protocol. *Radiat Meas* 32:57–73.
13. Galbraith RF, Roberts RG, Yoshida H (2005) Error variation in OSL palaeodose estimates from single aliquots of quartz: A factorial experiment. *Radiat Meas* 39: 289–307.
14. Bailey RM, Arnold LJ (2006) Statistical modelling of single grain quartz D_e distributions and an assessment of procedures for estimating burial dose. *Quat Sci Rev* 25:2475–2502.
15. Galbraith RF (2005) *Statistics for Fission Track Analysis* (CRC Press, Boca Raton, FL).
16. Rodnight H (2008) How many equivalent dose values are needed to obtain a reproducible distribution? *Ancient TL* 26:3–10.
17. Lepper K, McKeever SW (2002) An objective methodology for dose distribution analysis. *Radiat Prot Dosimetry* 101:349–352.
18. Fuchs M, Lang A (2001) OSL dating of coarse-grain fuvial quartz using single-aliquot protocols on sediments from NE Peloponnese, Greece. *Quat Sci Rev* 20:783–787.

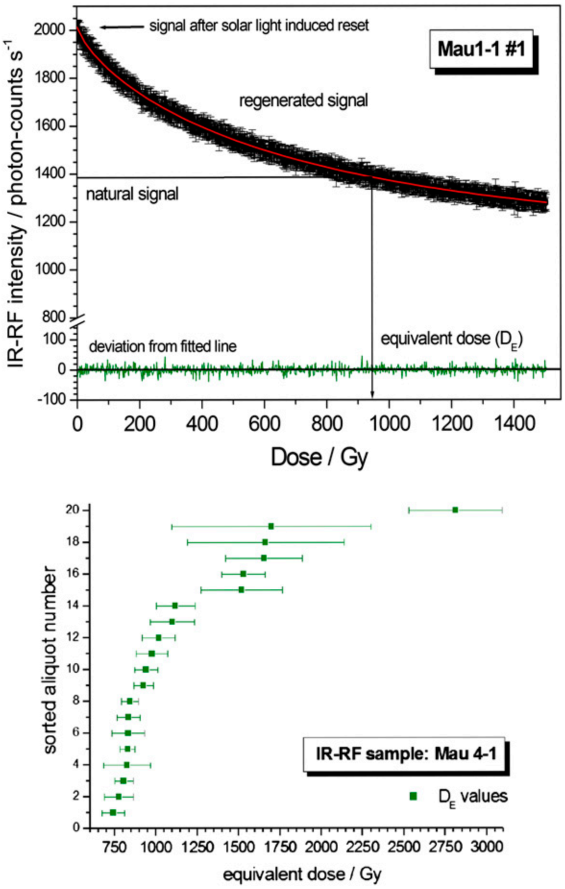

Fig. S1. Examples of equivalent dose determination using IR-RF of single aliquots. *Upper:* Measurement of an aliquot from sample Mau 1-1. The regeneration dose–response curve consists of 999 dose points. The residuals (deviation from fitted line) show good agreement with the stretched single exponential decay. A dose of 947 ± 82 Gy was determined. *Lower:* Single-aliquot equivalent doses of sample Mau 4-1. The values are sorted ascending.

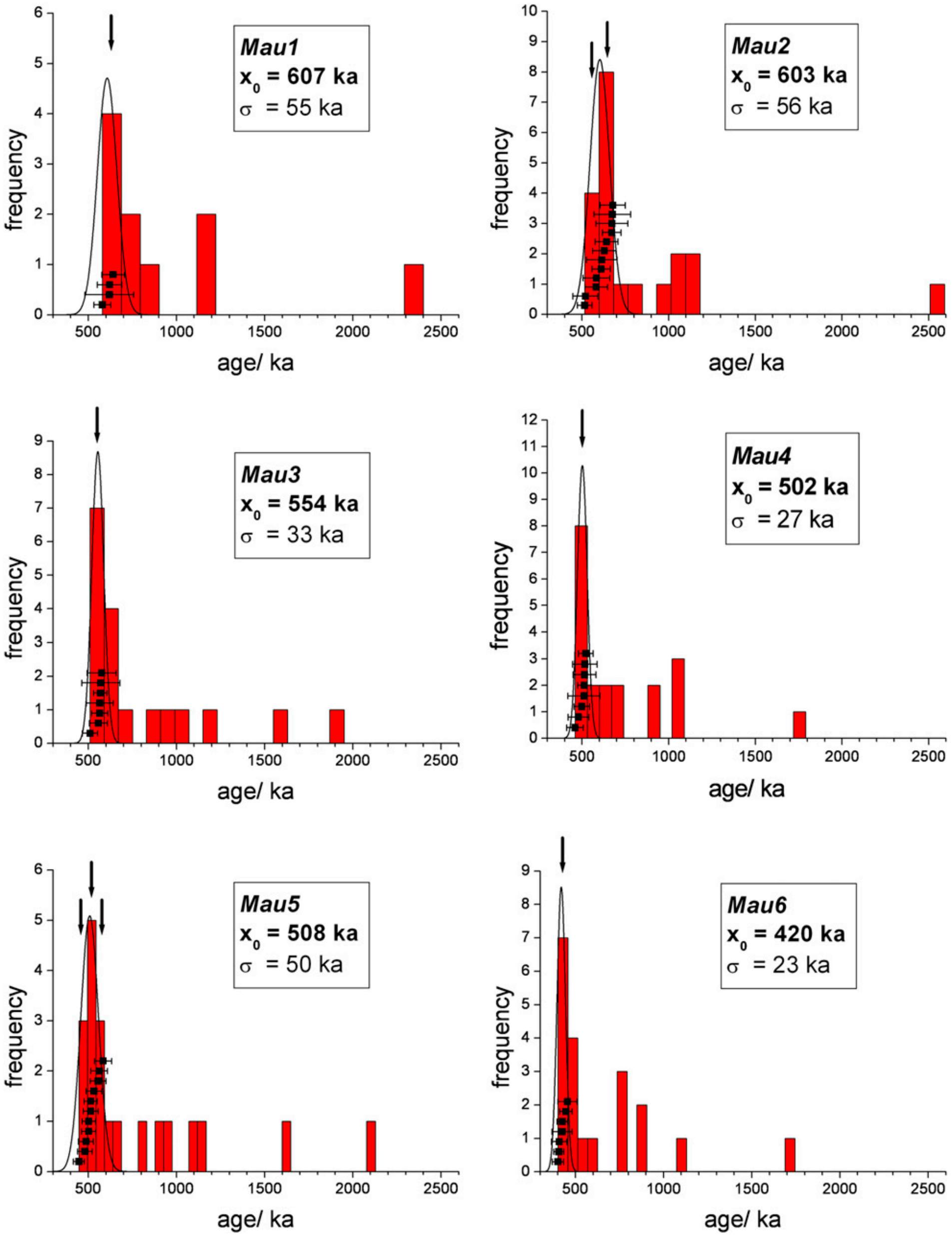

Fig. S2. Distribution of single-aliquot IR-RF ages and mean age for each sample. Normal distribution curves represent the well-bleached aliquots as described in *SI Materials and Methods*. Histogram bars, used for calculation of mean age, are marked by arrows.

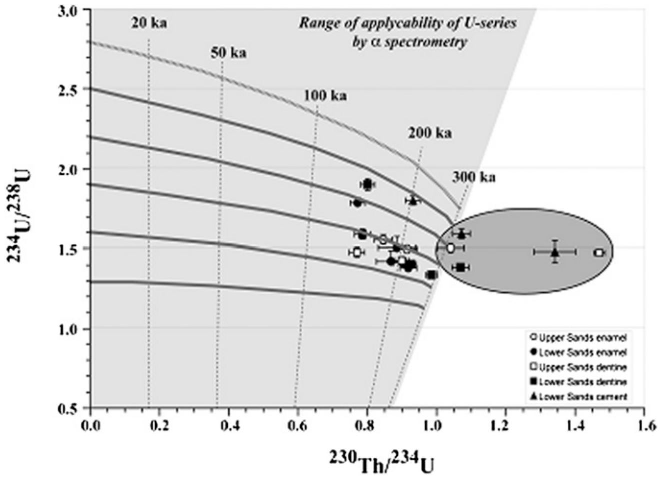

Fig. S3. U-series data obtained on the Mauer samples. The five tissues for which *P* values cannot be calculated are located in the ellipse in the right side of the scheme.

Table S1. Sediment moisture and radioisotope analyses by γ-spectrometry at two laboratories (error-weighted mean and SD)

	Moisture (in % dry mass)			γ-Spectrometry (Bq kg^{-1})		
Sample	In situ	Laboratory saturation	For age[*]	U	Th	^{40}K
Mau 1-1	2.8	25.6	18 ± 4	7.3 ± 0.2	7.3 ± 0.4	216.4 ± 1.3
Mau 1-2	2.9	23.6	17 ± 3	6.7 ± 0.2	7.0 ± 0.4	231.0 ± 1.4
Mau 1-1[†]				7.2 ± 0.3	8.5 ± 0.3	244.0 ± 12.0
Mean: Mau 1-1/-2				7.0 ± 0.1	7.7 ± 0.2	223.3 ± 1.0
Mau 2-1	2.6	25.4	18 ± 4	6.8 ± 0.2	6.5 ± 0.4	214.8 ± 1.4
Mau 2-2	3.9	26.2	19 ± 4	6.9 ± 0.2	6.7 ± 0.4	231.7 ± 1.5
Mau 2-1[†]				7.0 ± 0.3	8.2 ± 0.3	230.0 ± 12.0
Mean: Mau 2-1				6.9 ± 0.2	7.5 ± 0.2	215.0 ± 1.4
Mau 3-1	4.7	27.0	19 ± 4	5.7 ± 0.2	6.5 ± 0.4	241.2 ± 1.4
Mau 3-1[†]				8.7 ± 0.4	8.6 ± 0.3	294.0 ± 15.0
Mean: Mau 3-1				6.3 ± 0.2	7.7 ± 0.2	241.7 ± 1.4
Mau 4-1	4.7	28.6	21 ± 4	5.7 ± 0.2	6.9 ± 0.4	294.9 ± 1.7
Mau 4-1[†]				7.2 ± 0.3	8.8 ± 0.3	341.0 ± 17.0
Mean: Mau 4-1				6.2 ± 0.2	8.1 ± 0.3	295.4 ± 1.7
Mau 5-1	4.4	31.3	23 ± 5	8.2 ± 0.3	11.3 ± 0.6	387.4 ± 1.8
Mau 5-2	4.4	31.6	23 ± 5	8.7 ± 0.3	12.4 ± 0.6	403.3 ± 2.1
Mau 5-1[†]				10.6 ± 0.4	16.1 ± 0.5	467.0 ± 23.0
Mean: Mau 5-1				8.9 ± 0.2	14.0 ± 0.4	387.9 ± 1.8
Mau 6-1	5.5	34.8	25 ± 5	12.3 ± 0.3	18.1 ± 0.9	526.4 ± 2.2
Mau 6-2	5.2	33.9	24 ± 5	12.7 ± 0.4	19.2 ± 1.0	509.2 ± 2.6
Mau 6-1[†]				13.5 ± 0.5	21.5 ± 0.7	572.0 ± 29.0
Mean: Mau 6-1				12.7 ± 0.3	20.1 ± 0.5	526.7 ± 2.2

[*] For age calculation: natural saturation (= 0.9 of laboratory saturation) × 0.8 ± 0.2 (± SD, estimated).

[†] γ-measurements at Felsenkeller Laboratory Dresden.

Table S2. **Single-aliquot equivalent-dose *DE*, calculated mean cosmic dose rate, and sediment dose rate (SD, cosmic dose rate error: ±20% estimated)**

	DE (Gy)								
Single-aliquots (sorted)	Mau 1-1/-2	Mau 2-1	Mau 2-2	Mau 3-1_1	Mau 3-1_2	Mau 4-1	Mau 5-1	Mau 5-2	Mau 6-1
1	857 ± 56	837 ± 56	759 ± 72	844 ± 106	833 ± 56	743 ± 68	879 ± 37	963 ± 62	972 ± 56
2	917 ± 199	944 ± 94	851 ± 102	851 ± 155	913 ± 69	775 ± 88	947 ± 62	994 ± 49	984 ± 40
3	918 ± 92	990 ± 69	896 ± 120	859 ± 113	923 ± 58	806 ± 57	989 ± 59	1,016 ± 45	990 ± 91
4	947 ± 82	1,040 ± 93	918 ± 87	893 ± 102	929 ± 37	825 ± 143	1,010 ± 60	1,053 ± 64	1,030 ± 127
5	1,017 ± 108	1,090 ± 68	983 ± 123	952 ± 165	968 ± 79	829 ± 45	1,093 ± 63	1,112 ± 67	1,032 ± 46
6	1,104 ± 86	1,099 ± 103	985 ± 146	1,311 ± 162	978 ± 65	832 ± 98	1,185 ± 67	1,156 ± 71	1,082 ± 65
7	1,205 ± 185	1,239 ± 90	1,154 ± 169	1,735 ± 493	1,210 ± 93	835 ± 71	1,560 ± 229	1,263 ± 85	1,103 ± 117
8	1,662 ± 364	1,613 ± 187	1,528 ± 218	2,326 ± 1147	1,589 ± 152	843 ± 53	1,899 ± 190	1,739 ± 128	1,113 ± 75
9	1,741 ± 308	1,907 ± 221	1,621 ± 224		1,683 ± 131	925 ± 59	2,244 ± 293	2,144 ± 206	1,145 ± 80
10	3,499 ± 1425	4,120 ± 551	1,635 ± 303		3,113 ± 320	941 ± 70	3,211 ± 362	4,125 ± 337	1,177 ± 133
11						977 ± 96			1,214 ± 56
12						1,018 ± 99			1,278 ± 93
13						1,100 ± 134			1,464 ± 222
14						1,119 ± 117			1,799 ± 505
15						1,519 ± 247			1,880 ± 125
16						1,530 ± 130			1,901 ± 125
17						1,655 ± 231			2,079 ± 549
18						1,665 ± 473			2,104 ± 407
19						1,700 ± 602			2,604 ± 956
20						2,813 ± 281			4,181 ± 371
Grain-size (µm)	120–180	180–220	110–180	110–180	160–220	110–180	110–180	110–180	110–180
Moisture (calc.) %	18 ± 4	18 ± 4	19 ± 4	19 ± 4	19 ± 4	21 ± 4	23 ± 5	23 ± 5	25 ± 5
Cosmic (µGy a^{-1})	75 ± 15	78 ± 16	78 ± 16	78 ± 16	78 ± 16	78 ± 16	91 ± 18	91 ± 18	93 ± 19
Dose rate (mGy a^{-1})	1.48 ± 0.08	1.62 ± 0.08	1.46 ± 0.08	1.49 ± 0.08	1.63 ± 0.08	1.61 ± 0.08	1.97 ± 0.11	1.98 ± 0.11	2.42 ± 0.13

Table S3. IR-RF ages of each single aliquot for all samples (combined uncertainty from error propagation ± SE)

	Age (ka)					
No.	Mau 1	Mau 2	Mau 3	Mau 4	Mau 5	Mau 6
1	580 ± 48	516 ± 43	510 ± 43	460 ± 48	447 ± 31	401 ± 32
2	620 ± 138	520 ± 72	558 ± 51	480 ± 60	481 ± 41	406 ± 28
3	621 ± 70	582 ± 65	565 ± 45	499 ± 44	487 ± 42	408 ± 44
4	641 ± 65	583 ± 77	566 ± 77	511 ± 92	503 ± 41	425 ± 57
5	688 ± 81	611 ± 53	568 ± 37	514 ± 38	503 ± 38	426 ± 30
6	747 ± 70	614 ± 89	571 ± 108	515 ± 66	514 ± 42	446 ± 36
7	815 ± 132	629 ± 68	576 ± 82	517 ± 71	514 ± 37	455 ± 54
8	1,124 ± 253	642 ± 66	592 ± 57	522 ± 42	532 ± 44	459 ± 40
9	1,178 ± 217	672 ± 54	598 ± 50	573 ± 47	556 ± 45	472 ± 42
10	2,367 ± 972	673 ± 92	599 ± 75	583 ± 53	562 ± 47	485 ± 61
11		675 ± 106	639 ± 116	605 ± 67	584 ± 49	501 ± 36
12		678 ± 72	740 ± 68	631 ± 69	603 ± 48	527 ± 48
13		764 ± 68	879 ± 118	681 ± 90	639 ± 56	604 ± 97
14		790 ± 123	972 ± 105	693 ± 81	794 ± 125	742 ± 212
15		995 ± 126	1,030 ± 96	940 ± 160	879 ± 82	775 ± 67
16		1,057 ± 159	1,164 ± 336	948 ± 94	966 ± 111	784 ± 67
17		1,058 ± 156	1,560 ± 774	1,025 ± 152	1,084 ± 121	858 ± 231
18		1,120 ± 216	1,905 ± 218	1,031 ± 298	1,142 ± 162	868 ± 174
19		1,176 ± 149		1,053 ± 377	1,634 ± 205	1,074 ± 399
20		2,524 ± 363		1,743 ± 195	2,086 ± 208	1,725 ± 179

Table S4. List of the analyzed teeth samples

Sample laboratory no.	Excavation no.	Faunal species	Date of discovery	Geological unit	Depth vs. Lettenbank
M0501	M2198	*Stephanorhinus hundsheimensis*	April 1931	Lower sands	−5 m beneath
M0502	M2041	*Stephanorhinus hundsheimensis*	1934	Upper sands	+4 m above
M0503	M2373	*Bison schoetensacki*	1935	Lower sands	−6 m beneath
M0504	M2282	*Bison schoetensacki*	1935	Upper sands	0 m
M0505	M2337	*Bison schoetensacki*	1934	Upper sands	+2 m above
M0506	M2314	*Bison schoetensacki*	October 1932	Lower sands	−3 m beneath
M0507	M2345	*Bison schoetensacki*	October 1934	Lower sands	−4 m beneath
M0508	M2336	*Bison schoetensacki*	April 1931	Lower sands	−5 m beneath

Table S5. U-series data obtained from the Mauer analyzed teeth (±SEM)

Unit	Sample	Depth vs. Lettenbank	Tissue	U content (ppm)	^{234}U/^{238}U	^{230}Th/^{232}Th	^{230}Th/^{234}U	^{222}Rn/^{230}Th
Upper sands	M0502	+4 m	Enamel	1.10 ± 0.03	1.500 ± 0.028	>100	1.041 ± 0.039	0.583
			Dentin	106.56 ± 1.78	1.471 ± 0.021	>100	1.469 ± 0.016	0.300
	M0505	+2 m	Enamel	1.65 ± 0.04	1.552 ± 0.030	>100	0.847 ± 0.026	0.672
			Dentin	60.64 ± 1.32	1.474 ± 0.029	>100	0.771 ± 0.022	0.493
	M0504	+0 m	Enamel	1.07 ± 0.03	1.493 ± 0.024	25	0.915 ± 0.029	0.429
			Dentin	66.09 ± 1.25	1.423 ± 0.024	>100	0.900 ± 0.020	0.401
				Lettenbank				
Lower sands	M0506	−3 m	Enamel	1.24 ± 0.03	1.407 ± 0.030	>100	0.906 ± 0.030	1.000
			Dentin	66.69 ± 0.81	1.332 ± 0.015	>100	0.986 ± 0.016	0.354
			Cement	13.84 ± 0.54	1.477 ± 0.069	>100	1.341 ± 0.060	0.116
	M0507	−4 m	Enamel	2.98 ± 0.06	1.376 ± 0.022	>100	0.919 ± 0.024	0.310
			Dentin	66.54 ± 0.79	1.400 ± 0.015	>100	0.927 ± 0.015	0.314
	M0508	−5 m	Enamel	0.54 ± 0.02	1.502 ± 0.070	>100	0.886 ± 0.054	0.300
			Dentin	51.77 ± 1.16	1.586 ± 0.031	>100	0.787 ± 0.023	0.337
			Cement	32.18 ± 0.65	1.589 ± 0.031	>100	1.072 ± 0.025	0.235
	M0501	−5 m	Enamel	0.43 ± 0.02	1.417 ± 0.066	35	0.869 ± 0.042	0.841
			Dentin	50.75 ± 0.92	1.380 ± 0.021	>100	1.069 ± 0.024	0.321
	M0503	−6 m	Enamel	1.23 ± 0.03	1.782 ± 0.033	>100	0.773 ± 0.021	1.000
			Dentin	70.42 ± 1.56	1.896 ± 0.037	>100	0.802 ± 0.020	0.493
			Cement	39.33 ± 0.71	1.797 ± 0.028	>100	0.932 ± 0.021	0.239

Table S6. Electron spin resonance data for the Mauer analyzed teeth (±SEM)

						Dose rate (μGy/a)			
Unit	Sample	Depth vs. Lettenbank	Enamel initial thickness (μm)	Removed enamel thickness dentin side (μm)	Removed enamel thickness cement or sediment side (μm)	Internal α + β enamel	External β	External γ + cosmic	Total
Upper sands	M0502	+4 m	1,966 ± 246	349 ± 44	114 ± 14	656 ± 77	785 ± 123	647 ± 47	2,088 ± 136
	M0505	+2 m	1,258 ± 157	143 ± 18	106 ± 13	416 ± 114	241 ± 53	645 ± 44	1,404 ± 134
	M0504	+0 m	1,242 ± 155	105 ± 13	147 ± 18	265 ± 75	495 ± 121	745 ± 52	1,504 ± 140
Lettenbank									
Lower sands	M0506	−3 m	1,152 ± 144	54 ± 7	238 ± 13	303 ± 124	848 ± 328	330 ± 21	1,478 ± 288
	M0507	−4 m	1,190 ± 149	183 ± 23	101 ± 13	594 ± 176	385 ± 98	327 ± 20	1,305 ± 199
	M0508	−5 m	1,156 ± 145	109 ± 14	79 ± 10	47 ± 37	717 ± 267	332 ± 20	1,095 ± 214
	M0501	−5 m	1,258 ± 157	143 ± 18	106 ± 13	98 ± 73	607 ± 13	332 ± 20	1,037 ± 202
	M0503	−6 m	1,330 ± 166	155 ± 19	159 ± 20	267 ± 70	483 ± 155	330 ± 19	1,080 ± 133